Volume 1 | Number 1 | Jan 2013 | Pages 1–100

Journal of
Materials Chemistry A

Materials for energy and sustainability
www.rsc.org/materialsA

Li⁺

ROYAL SOCIETY
OF CHEMISTRY

ROYAL SOCIETY
OF CHEMISTRY

www.rsc.org/materialsA

Synthesis of flower-like CuS hollow microspheres based on nanoflakes self-assemble and their microwave absorption properties

Biao Zhao [a], Gang Shao [a] *, Bingbing Fan [a], Wanyu Zhao [a], Yajun Xie [a], Rui Zhang [a, b] *

ABSTRACT: Flower-like CuS hollow microspheres composed of nanoflakes have been successfully prepared via a facile solvothermal method. The crystal structure, morphology and microwave absorption property of the as-synthesized products are characterized by X-ray diffraction (XRD), scanning electron microscopy (SEM), transmission electron microscopy (TEM) and network analyser. The effects of reaction temperature, concentration of the reagents and reaction time on the structures and morphologies of CuS 10 products were investigated by the assistance of XRD and SEM techniques. A plausible mechanism for the formation of hollow architectures related to Ostwald ripening was proposed. The CuS/paraffin composite containing 30 wt% CuS hollow microspheres shows the best microwave absorption properties compared with other CuS/paraffin composites. The minimum reflection loss of −31.5 dB can be observed at 16.7 GHz and reflection loss below -10 dB is 3.6 GHz (14.4-18.0 GHz) with only thickness of 1.8 mm. The effective absorption (below -10 dB, 90% microwave absorption) bandwidth can be tuned between 6.2 GHz and 18.0 GHz for the absorber with the 15 thin thickness in 1.5−4.0 mm. The results implies that the microwave absorption properties of flower-like CuS hollow microspheres which possess the advantages of broad bandwidth, strong absorption, light weight and thin thickness are superior to those of other absorbing materials.

1. Introduction

20 Nowadays, with the expandable usage of microwave wave circuit devices in commercial, industrial, and military applications at high-frequency, the serious electromagnetic interference (EMI) problems have become a great issue in both military and civil applications.[1-5] EMI not only impedes the 25 functionality of electronic devices but also harms the health of human being. The great efforts have been devoted toward exploiting absorbing materials, which can absorb unwanted electromagnetic wave energy impinged onto the surface and transform it into heat and/or other types of energy. [6-8] It is well 30 known that the complex permittivity, complex permeability, the electromagnetic impedance match, and the microstructure of the absorber determine their microwave absorption properties. [9] Microwave absorbing materials are now supposed to have the features of lightweight, thin thickness, wide absorption 35 bandwidth, strong absorption and simple operation. [10-12]

Among the candidates for the microwave absorption, the materials with hollow structure hold the advantages of high surface area and light-weight over the other absorbing materials, which have attracted intensive attention.[13, 14] Deng et al. prepared 40 submicrometer-sized nickel spheres and the minimum reflection loss of −34.5 dB was observed at 12.0 GHz with the thickness of 2.0 mm. [15] Low density composite powders of hollow microsphere/titania/M-type Ba ferrite were prepared using a two-step sol-gel technique by Mu et al. [16] and the minimum reflection 45 loss is −30.1 dB at 8.5 GHz with a thickness of 2.4 mm. Shi et al. reported the synthesis of hollow Co nanochains and the minimum reflection loss was −17 dB at 17.5 GHz with a thickness of 3.0 mm. [17] Liu et al. described the synthesis of porous carbon/Co nanocomposites and the maximum reflection 50 loss of the porous C(Co) nanocomposite can reach 40 dB at 4.2 GHz with 5 mm. [18] Cao et al. synthesized the hollow CdSe nanospheres by a ligand-assisted solvothermal method and also investigated their microwave absorption properties. [19] Based on above results, hollow materials are recognized as the most 55 promising microwave absorbers because of their excellent properties, such as low density, large specific surface area, and high energy absorption. [20] Therefore, to select a novel hollow materials with the features of light-weight, strong absorption, thin-thickness and wide-band is very meaningful and urgent.

60 Copper sulfide (CuS), as one of the most important semiconductor transition-metal chalcogenides, has been studied

intensely. [21-23] CuS possesses excellent optical, electronic and other physical and chemical properties with the great potential applications in the fields of lithium storage, high-capacity cathode material in lithium secondary batteries, photocatalyst, supercapacitors and optical sensors. [24-27] Moreover, it is well known that topological structure is a vital parameter affecting nanomaterial performance. CuS nanoparticles with various structures of nanorods, nanotubes, concave superstructures, nanoplates, nanowire arrays and flowers have been reported as well as their relative properties. [28-32] More recently, the microwave absorption properties of CuS materials have also been performed by some groups. [33-35] CuS hexagonal platelet and complex symmetrical CuS nanostructures have been successfully synthesized and their CuS/PVDF composites exhibits the outstanding microwave absorption properties. However, their weight were too heavy to apply in the electromagnetic wave absorption. On the other hand, to the best of our knowledge, there are no literatures about the microwave absorption performances of hollow CuS. In current work, the flower-like hollow CuS architectures were synthesized through a facile solvothermal method. The microwave absorption properties of flower-like hollow CuS microspheres based on nanoflakes self-assemble were also investigated in the frequency of 1-18 GHz. The electromagnetic wave absorption properties of flower-like hollow CuS microspheres shows the features of lightweight, strong absorption, thin thickness and wide-band, which meets the current requirement of absorbing materials. From this view, this work is competitive.

2. Experimental section

All reagents, such as copper sulfate pentahydrate ($CuSO_4 \cdot 5H_2O$, AR), cetyltrimethyl ammonium bromide (CTAB, AR) and sulfur powder (S, AR), were purchased from commercial suppliers and used without any further purification.

2.1 Preparation of hollow CuS hierarchical structures

Typically, at room temperature, ethylene glycol (EG, 60 ml) was used as the starting solvent. Firstly, 0.001mol $CuSO_4 \cdot 5H_2O$ and 0.001 mol CTAB was added to 60 ml ethylene glycol with magnetic stirring. Then 0.002 mol sulfur powder was introduced to this system, and kept stirring for 30 min to create a steady solution. Finally, this mixture solution was transferred into a Teflon-lined stainless steel autoclave and then the autoclave heated and maintained at 160°C for 15 h. After the reaction, the solution was cooled to room temperature, and then washed with distilled water and absolute ethanol several times and dried at 60 °C for 12 h.

2.4. Characterization. The morphology of the as-prepared samples was observed by field-emission scanning electron microscope (FESEM, JEOL JSM-7001F). The element composition of the samples was characterized by energy dispersive spectrometer (EDS, Oxford Instruments), associated with FE-SEM. The phase structures of the samples were analyzed by X-ray diffraction (XRD, XD-3, Cu Kα radiation, λ =1.54178 Å. Beijing Purkinje General Instrument Co. Ltd). Transmission electron microscopy (TEM) images and high-resolution TEM (HRTEM) investigations were captured on the JEOL JEM-2100F microscope. The hollow CuS/paraffin composite samples were prepared by uniformly blending the flower-like hollow CuS microspheres in a paraffin matrix which was considered as binder and then pressing the mixture into a cylindrical-shaped compact with the outer diameter of 7.00 mm, the inner diameter of 3.04 mm. The scattering parameters of the toroidal-shaped samples were measured using a network analyzer (Agilent N5244A). The relative complex permeability ($\mu_r = \mu - j\mu''$) and permittivity ($\varepsilon r = \varepsilon' - j\varepsilon''$) values were determined from the scattering parameters in the frequency range of 1.0-18.0 GHz.

3. Results and discussion

A typical powder X-ray diffraction (XRD) pattern of the as-synthesized hollow CuS microspheres is shown in Fig. 1a. All diffraction peaks of the product can be well assigned to a pure hexagonal phase of CuS (JCPDS no. 06-0464). No additional peaks for other phases were observed, thus indicating high purity and crystallinity of the products. EDS analysis of composite microspheres indicates that the obtained hollow CuS microspheres are composed of Cu and S elements (Fig.1b). The C

element signal originates from the carbon conductive tape to support the samples during the test and O peaks are assigned to the oxygen residual or oxide in the composite, which is in good agreement with the XRD analysis. From XRD and EDS patterns, [5] one can conclude that the hollow CuS microspheres obtained by this method consist of a pure phase.
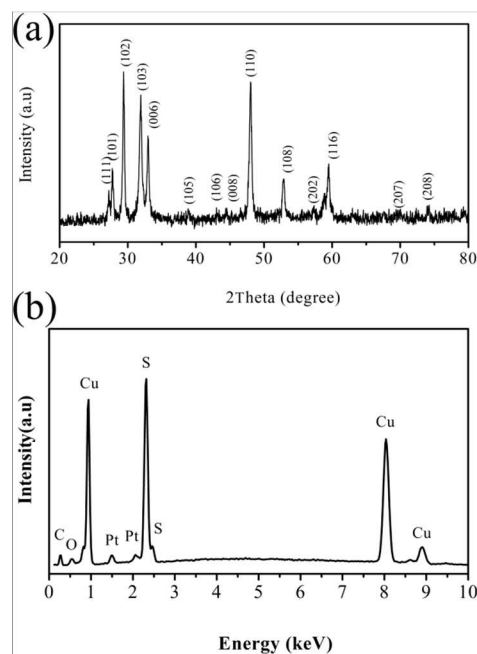

Fig. 1 (a) XRD pattern and (b) EDS profile of the hollow CuS hierarchically microspheres.
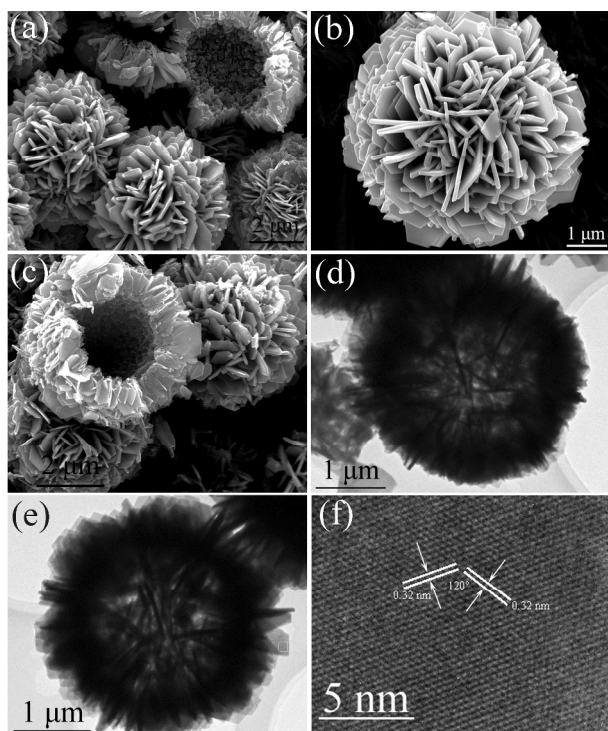

Fig. 2 (a-c) Different magnification FESEM views, (d,e) TEM and (f) HRTEM image of hollow CuS hierarchical structures by nanoflake self-assembly prepared at 160 °C.

The morphology and structure of the hollow CuS [15] hierarchical architectures are characterized by SEM, TEM and HRTEM. Fig. 2a is a typical low-magnification SEM image of the as-synthesized product, which clearly reveals hierarchical flower-like microspheres with the diameter of ~3 μm. Further observation from high magnification SEM (Fig. 2b) indicates that [20] the flower-like microsphere is comprised of nanoflakes self-assemble with a thickness of about 10 nm. Interestingly, some CuS microspheres display broken sites and reveal their hollow interiors (Fig.2a,c), which provides direct evidence that the CuS microspheres possess hollow structures. Further characterization [25] of the flower-like architectures is obtained from the TEM images. Fig. 2d and 2e show two typical TEM images of the hollow CuS architectures, with an average diameter of 3 μm. The contrast between the dark edge and the pale centre shown in the TEM image is also evidence of the hollow nature of the microspheres, [30] in accordance with the SEM observations. The TEM images also reveal that the microsphere is constructed by many nanoflakes. Fig. 3f shows the HRTEM images of the hollow CuS architectures. It can be observed that the lattice spacing is 0.32 nm, which is corresponding to the distance between the {102} [35] lattice planes, thus indicating the single-crystalline nature of the CuS nanoflakes.

Generally, the reaction temperature plays an important role in determining the morphology of the products. We have systematically investigated this system with reaction temperatures [40] in the range of 120–180°C and the XRD patterns and SEM images of the products obtained at different reaction temperatures are shown in Fig. S1. When the reaction temperature was decreased from the typical temperature (160°C) to 120°C, uniform dense microspheres with the diameter of 3-4 μm and [45] some nanoflakes grown on the microspheres were obtained (Fig.S1b). The XRD pattern of dense microspheres, as shown in Fig.S1a, can be indexed to a mixture of S and CuS. With the

increase of reaction temperature to 140°C, the obtained products are mainly composed of dense flower-like microspheres built from thin nanoflakes (Fig.S1c). The corresponding XRD pattern is shown in Fig. S1a, where only hexagonal phase of CuS (JCPDS no. 06-0464) exists in this case. The SEM images (Fig. 2 and Fig. S1d) and XRD patterns (Fig. 1 and Fig. S1a) show that the flower-like CuS hollow microspheres composed of nanoflakes are produced at temperatures ranging from 160 to 180°C. The products obtained at different reaction temperatures illustrate that sulfur are remained at low reaction temperatures and will be completely converted into CuS microspheres with increasing reaction temperatures.

Fig.S2 shows the XRD patterns and SEM images of CuS products prepared at different molar ratios of $CuSO_4$:S (1:6, 1:4, 1;1). As shown in Fig.S2a, the final products consist of mixture phases of S and CuS when the high concentration of sulfur was introduced into this system (1:6). The peaks of S in XRD pattern are observed, which may be due to residual S during the solvothermal reaction. In the solothermal reaction process, the excess S would undergo the process of sublimation, condensation and then deposit on the surfaces of CuS products, coexisting with CuS. As shown in inset of Fig.S2b, S remains were marked by the arrows, which can be clearly seen that dense S deposited on the CuS hierarchical microsphere. With decreasing the concentration of sulfur (1:4, 1:1), only CuS crystals were observed in products. In this reaction, R (the molar ratio of $CuSO_4 \cdot 5H_2O$/S) is also an important factor that affects the morphology of the prepared product. When R is 1:6, the products were composed of spherical architectures and some disperse nanoflakes. Moreover, spherical architectures contain pores on the surfaces (Fig.S2b). When the molar ratio changed to 1:4, the amount of nanoflakes increased, and hollow architectures are also observed in the sample (Fig.S2c). When the molar ratio increased to 1 : 1. The flower-like core/void/shell CuS architectures can be observed in the products (Fig.S2d). From the above mentioned, R not only influences the phase and morphology of CuS products but also affects the reaction system.

To further disclose the growth mechanism of flower-like hollow CuS microspheres, Products were collected at reaction times of 1, 6, 12 and 15 h and their phases and morphologies were evaluated by XRD and SEM techniques, as shown in Fig. S3 and Fig. 3, respectively. From the Fig.S3, it can be found that all diffraction peaks of the products prepared at various reaction times could be well assigned to CuS phases, which indicates that the CuS nanocrystals were formed at the beginning reaction time. Moreover, with increasing the reaction time, the XRD pattern of the product obtained became much sharper, which indicates the crystallinity increases with increasing reaction time.
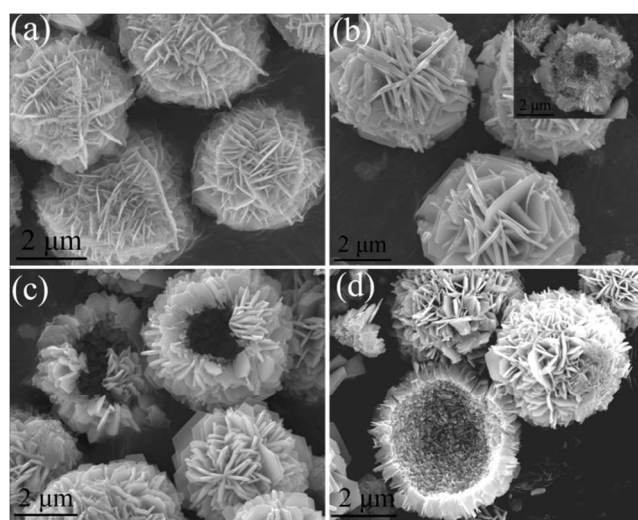

Fig. 3 FESEM image of the products obtained at 160°C under different reaction times: (a) 1 h, (b) 6 h, (c) 12 h, and (d) 15 h. The inset of (b) is the enlarge FESEM image of products prepared at 6 h.

Fig. 3a–d displayed the SEM images of the synthesized CuS samples prepared at various reaction times from 1 to 15 h. When the reaction time was 1 h, relatively uniform dense flower-like microspheres were obtained, mainly flake-like crystals growing on the surface of microspheres (Fig. S3a). While the reaction time was prolonged to 6 h, the nanoflakes gradually become big and thick. Meanwhile, inner CuS products were dissolved and form shell-shell-void unique structures (Fig.3b). As the hydrothermal time increased to 12 h, the crystal size of the 3D hierarchical CuS nanostructure grew gradually. Simultaneously, hollow flower-like CuS architectures were formed, as shown in Fig.3c. Finally, well-

defined 3D hierarchical flower-like hollow nanostructures were obtained after prolonging the reaction time to 15 h (Fig.3d). Hence, it can be deduced that the reaction time played a critical role in controlling the final morphology of CuS products.
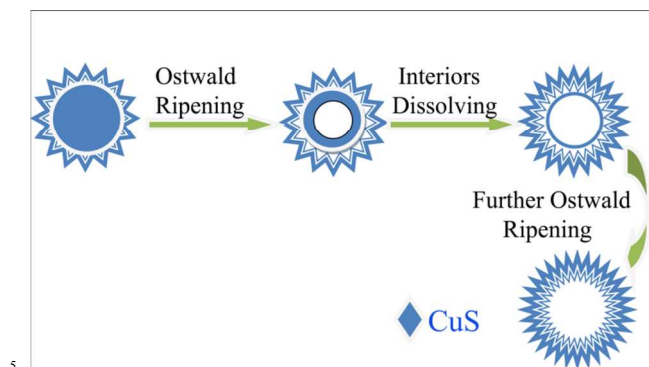

Fig. 4 Schematic illustration for the formation of flower-like hollow CuS hierarchical microspheres.

According to the above experimental results, the formation mechanism of the flower-like CuS hollow microspheres could be attributed to the Ostwald ripening process.[19, 36-38] The Ostwald ripening contains the growth and recrystallization given a sufficient ripening time. Fig.4 illustrates the whole morphology evolution process based on Ostwald ripening. On the basis of this mechanism, firstly, dense microspheres were formed and some nanflakes were grown on the surfaces of microspheres due to minimization of their surface energies by an oriented attachment. In the present case, CTAB is an effective surfactant, [33, 39, 40] which plays a crucial role in the formation of the flake-like structure. In order to investigate the effect of CTAB on the morphology of CuS products, the CuS sample without adding CTAB was also prepared with other preparation parameters unchanged. Fig. S4 shows the FESEM images of CuS products prepared without adding CTAB. A general SEM overview of the as-prepared product is shown in Fig. S4a. The products are mainly complex symmetrical microstructures which are totally different with those of adding CTABA samples. An enlarged image (Fig. S4b) shows the diameters of the flakes are about 3.0 μm with thicknesses around 300 nm. Subsequently, via Ostwald ripening, the central cavity is created, accompanied by the growth of larger outer nanoflake crystallites at the expense of inner ones.

As the reaction proceeded, to reduce the total surface energy, the inner crystallites further dissolved and transferred out, producing shell-shell-void hollow microspheres. With further increase in the reaction time, the cores in the centre could be completely consumed and the final hierarchical hollow flower-like structures were fabricated.
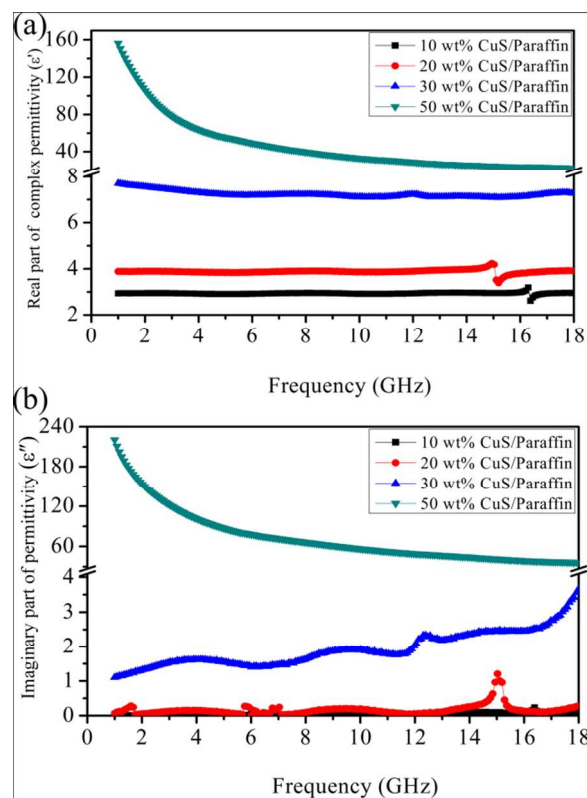

Fig. 5 Frequency dependence on real parts (a) and imaginary parts (b) of the complex permittivity of paraffin-composites containing different CuS loadings.

To investigate how the hierarchical CuS microspheres disperse in the paraffin-composites, various amounts of hollow CuS flowers are mixed with paraffin wax to form CuS paraffin-composites. The SEM images of the paraffin composite with 30wt% in Fig. S5 shows good dispersion of the hollow CuS flowers in the paraffin matrix. The hollow CuS complex microspheres are kept in the composites (Fig.S5b). In terms of the features of microwave absorbers, the flower-like hollow CuS microspheres should exhibit outstanding microwave absorbing properties. Owing to the absence of magnetic constituents in the hierarchical hollow microspheres, the real part (μ') and imaginary

part (μ″) of complex permeability are about 1.0 and 0.0, respectively (not shown). In the relative complex permittivity, the real part (ε′) and imaginary part (ε″) symbolize the storage and loss capability for electromagnetic wave energy, respectively. [41-43] Fig. 5 exhibits the frequency-dependent real (ε′) and imaginary (ε″) parts of the complex permittivity of the CuS paraffin-composites with various CuS loadings. It can be found that the ε′ values increase with increasing CuS loadings (Fig.5a). For the imaginary part (ε″), it also presents the same increase trend compared with real part (ε′) (Fig.5b). When the loading of CuS was 30 wt%, the real permittivity was around 8, which is 2 times higher than that of the loading of 20 wt% CuS. Meanwhile, the ε″ values is about 10 times higher than that of the loading of 20%wt CuS, which indicates high conductivity and high dielectric loss. It may be due to the formation of 3D interconnected conductive network and intrinsic dielectric properties of the CuS microspheres. However, with further increasing the loading of CuS to 50 wt%, the ε′ and ε″ of CuS paraffin-composite show the highest values compared with other three CuS paraffin-composite, which means this paraffin-composite might possess the outstanding microwave absorption properties. However, the impedance match should be considered, [34, 44, 45] which require the complex permittivity should be close to complex permeability. Too high complex permittivity might lead to impedance mismatch, which is harmful to the microwave absorption properties and most incident microwaves will be reflected from the surfaces of absorber rather than absorption.[46] Thus the complex permittivity should be controlled in a rational range.

According to the free electron theory, [47, 48] $\varepsilon'' \approx 1/\pi\varepsilon_0\rho f$, where ρ is the resistivity, high ε″ means high conductivity. For the CuS paraffin-composite with 30 wt% CuS, highly complex nonlinear resonant behavior can also be observed in the ε″ curve. [49] Similar multiresonance behaviors can also be found in ZnO architectures. [50-52] This resonance behavior is generally associated with highly conductive and skin effects, [52] electronic spin and charge polarizations due to point effects, and with polarized centers. [53] In this work, the enhanced multiresonance peaks are attributed to the conductive CuS networks that gradually form in the paraffin matrix as the mass fraction increases. Furthermore, the flower-like CuS hollow microspheres composed of nanoflakes with special structures can generate additional interfacial polarization and/or orientation polarization.[54]

To evaluate the electromagnetic wave absorption ability, which is commonly denoted by the reflection loss (RL), could be simulated on the basis of the relative permeability and permittivity for a given frequency and absorber thickness, by means of the following equations: [55-58]

$$RL = 20\log_{10}\left|(Z_{in} - Z_0)/(Z_{in} + Z_0)\right| \qquad (1)$$

$$Z_{in} = Z_0\sqrt{\frac{\mu_r}{\varepsilon_r}}\tanh\left(j\frac{2\pi fd\sqrt{\mu_r\varepsilon_r}}{c}\right) \qquad (2)$$

Where Z_0 is the impedance of free space, Z_{in} is the input characteristic impedance, ε_r is the complex permittivity, μ_r is the complex permeability, f is the frequency, c is the velocity of light, and d is the thickness of the composites. Thus, the theoretical reflection loss (RL) of the CuS/paraffin with filler loading of 10 wt%, 20 wt%, 30 wt% and 50 wt% at a thickness of 2.0 mm can be obtained through eqn (1) and (2) (shown in Fig. 6a). It can be seen that the CuS/paraffin with 30 wt% CuS show the strongest microwave absorption properties among four CuS paraffin composites. The minimum reflection loss of -29.1 dB at 15.1 GHz. The RL values less than -10 dB (90% microwave attenuation) were observed in the 12.8-17.5 GHz rang with only absorber thickness of 2.0 mm. In the low filler concentration (10 wt%, 20 wt%), the hollow CuS microspheres are highly dispersed in the paraffin matrix, in which the CuS can not connect with each other and conductive CuS networks could not produce. When the high concentration of CuS (50 wt%) was introduced in the wax-matrix, too high complex permittivity leads to impedance mismatch and more incident microwave are reflected on the surface of absorbers. Based on the above equations, it can be known that the thickness of microwave absorber also plays an important role in determining the microwave absorption properties. The calculated theoretical reflection loss of the CuS/paraffin composites with various thicknesses (1.5– 4.0 mm)

in the range of 1– 18 GHz with the loadings of 30 wt% CuS was shown in Fig.6b. The optimal reflection loss is –31.5 dB at 16.7 GHz and RL below -10 dB is 3.6 GHz (14.4-18.0 GHz) with the only thickness of 1.8 mm. The effective absorption (below -10 dB) bandwidth can be adjusted between 6.2 GHz and 18.0 GHz for the absorber with the thin thickness in 1.5−4.0 mm. It can be found that the attenuation peaks would shift to lower frequencies and two RL peaks appear with the increasing thickness. Such phenomenon can be well described by the quarter-wavelength cancellation model that the incident and reflected waves in the absorber are out of phase 180°, which lead to the reflected waves in the air-absorber interface totally cancelled.[59, 60] For comparison, the microwave absorption properties of dense CuS spheres synthesized at 120 °C (Fig. S1b) were also investigated. Fig. S6 depicts the electromagnetic parameters (ε', ε'' and tan $\delta\varepsilon$) and reflection loss of dense CuS spheres obtained at 120 °C. Compared with hollow flower-like CuS, it can be obviously seen that the dense CuS microspheres exhibit weak microwave absorption capabilities with a minimal reflection loss of -4.3 dB only.
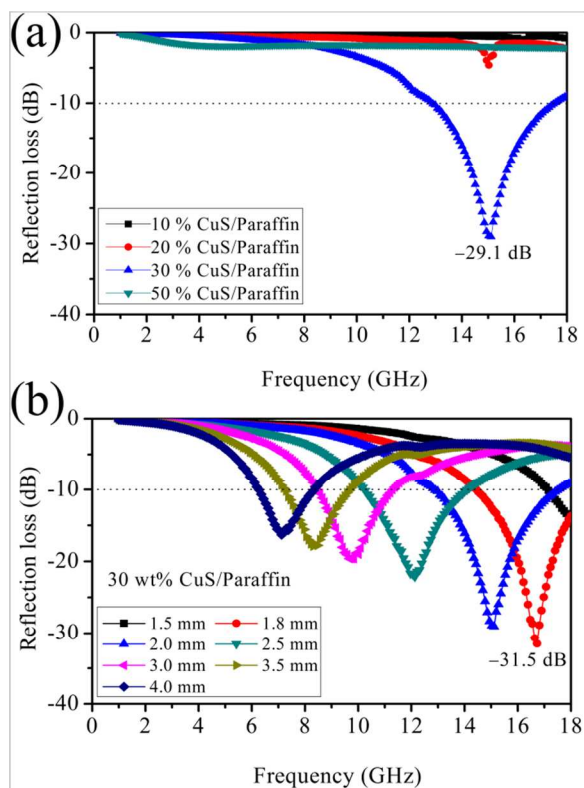

Fig. 6 (a) Microwave RL curves of the composites with a thickness of 2.0 mm in the frequency range of 1–18 GHz; (b) Reflection loss calculated for the CuS–paraffin composite absorbers containing 30wt% CuS loading with the various thicknesses.
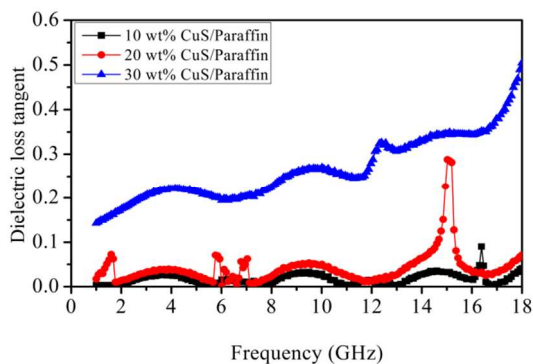

Fig. 7 The dielectric loss tangent for the CuS/paraffin composite with different CuS loadings.

The dielectric loss tangent (tan δ_ε = $\varepsilon''/\varepsilon'$) of the filled paraffin composites are closely related to the dielectric relaxation of the particulate fillers. The bound electrons of dielectric nanocrystallines will migrate in an alternating electromagnetic field to form relaxation and orientation polarization and loss, inducing dielectric loss. [41] The dielectric loss tangent of CuS/paraffin composites with different loadings (as showed in Fig. 7) was calculated in the term of complex permittivity from Fig.5. It can be found that the dielectric losses of the paraffin-composites are increased with increasing the CuS concentration and frequency, which is in accordance with the ε'' curve (Fig.5b). Therefore, in the appropriate range of filler concentration, the increasing loading of CuS results in enhancement of the dielectric loss.
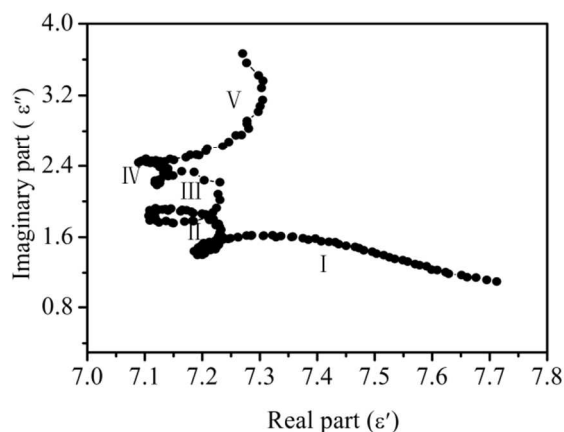
Fig. 8 The relation between real part (ε′) and imaginary part (ε″) of the CuS paraffin-composite with 30 wt% CuS.

For the dielectric loss of microwave absorbing materials, Debye dipolar relaxation is an important mechanism, which can account for the dielectric loss. The relative complex permittivity ε_r can be expressed by the following equation:[35, 61-64]

$$\varepsilon_r = \varepsilon_\infty + \frac{\varepsilon_s - \varepsilon_\infty}{1 + j2\pi f\tau} = \varepsilon' - j\varepsilon'' \tag{3}$$

In which ε_s, ε_∞, f, τ are the static permittivity, relative dielectric permittivity at the high-frequency limit, frequency and polarization relaxation time, respectively. Thus, ε′ and ε″ can be described by

$$\varepsilon' = \varepsilon_\infty + \frac{\varepsilon_s - \varepsilon_\infty}{1 + (2\pi f)^2 \tau^2} \tag{4}$$

$$\varepsilon'' = \frac{2\pi f\tau(\varepsilon_s - \varepsilon_\infty)}{1 + (2\pi f)^2 \tau^2} \tag{5}$$

based on eqn (2) and (3), the relationship between ε′ and ε″ can be deduced

$$\left(\varepsilon' - \frac{\varepsilon_s - \varepsilon_\infty}{2}\right)^2 + \left(\varepsilon''\right)^2 = \left(\frac{\varepsilon_s - \varepsilon_\infty}{2}\right)^2 \tag{6}$$

Thus, the plot of ε′ versus ε″ would be a single semicircle, generally regarded as the Cole–Cole semicircle.[65] Each semicircle refers to one Debye relaxation process. Fig. 8 exhibits the ε′-ε″ curve of CuS/paraffin composite with 30 wt% CuS. Five semicircles were found in the curve of the CuS/paraffin composite, which indicates that the Debye relaxation process is helpful to the enhancement of dielectric properties of the

CuS/paraffin. However, the Cole–Cole semicircles are distorted, indicating that besides the Debye relaxation, other mechanisms such as the Maxwell–Wagner relaxation, electron polarization and dipolar polarization are also existed in this composite. [66] In CuS paraffin-composites, the multi-interfaces between the CuS powders, paraffin matrix, and air bubbles can benefit the microwave absorption because of the interaction of electromagnetic radiation with charged multipoles at the interfaces. [67] The Interfacial polarization [18, 68] always takes place in materials comprised of more than one phase composites. This polarization occurring at the interfaces is due to the migration of charge carriers through different dielectric properties of the composite material, which results in charge accumulation at the interfaces. During the activation of an electromagnetic wave, an additional interfacial relaxation is produced, which is beneficial for the microwave absorption. Moreover, the unique flower-like hollow structures of CuS also make contribution to the microwave attenuation. Flake-like CuS can act as microwave receiver, which is easy for the electromagnetic wave to penetrate the surfaces of absorbers and enter into the absorbing materials.[69] Otherwise, when the sample was placed under the radiation of electromagnetic wave, the microwave penetrated CuS shell into the inner hollow space. It can lead to multiple reflection and diffuse scattering of the incident microwaves (Fig.9), which results in the attenuation of electromagnetic (EM) energy. [70, 71]
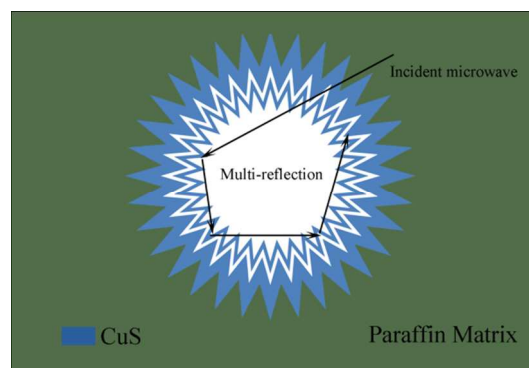

Fig.9 A possible mechanism of the microwave absorption in flower-like hollow CuS/paraffin composite.

4. Conclusion

In summary, the flower-like hollow CuS architectures comprised of nanoflakes have been synthesized by a solvothermal method. The effect of the reaction conditions, including reaction temperature, concentration of reactants and reaction time on the morphology of CuS was systematically investigated. The results show that the reaction temperature and the concentration of the reactants play a crucial role in the formation of flower-like CuS hollow microspheres. The formation mechanism of the flower-like CuS hollow microspheres is associated to the Ostwald ripening process, based on the time-dependent experiments. The microwave absorption properties of hollow CuS/paraffin composite were investigated in the frequency of 1-18 GHz. In the CuS/paraffin composite with 30 wt% CuS, the hollow structures consist of small nanoflakes building blocks that endow them with a higher electrical conductivity and accordingly results in enhanced microwave absorption properties. The optimal reflection loss (RL) is –31.5 dB at 16.7 GHz and RL below -10 dB is 3.6 GHz (14.4-18.0 GHz) with the only thickness of 1.8 mm. These hollow architectures potentially hold promise as microwave absorbers with the features of light-weight, strong-absorption, thin-thickness and wide-band.

Acknowledgements

Notes and references

a School of Materials Science and Engineering, Zhengzhou University, Zhengzhou 450001, China

b Laboratory of Aeronautical Composites, Zhengzhou Institute of Aeronautical Industry Management, Zhengzhou 450046, China

* Corresponding Author.

Dr. Gang Shao

E-mail address: gang_shao@zzu.edu.cn

Prof. Rui Zhang

Tel: +86-371-60632007

Fax: +86-371-60632600

E-mail address: zhangray@zzia.edu.cn

1. J. Jiang, D. Li, D. Geng, J. An, J. He, W. Liu and Z. Zhang, *Nanoscale*, 2014, **6**, 3967-3971.

2. Z. Yu, N. Zhang, Z. Yao, X. Han and Z. Jiang, *J. Mater. Chem. A*, 2013, **1**, 12462-12470.

3. L. Kong, X. Yin, Y. Zhang, X. Yuan, Q. Li, F. Ye, L. Cheng and L. Zhang, *J. Phys. Chem.C*, 2013, **117**, 19701-19711.

4. Y. Li, J. Zhang, Z. Liu, M. Liu, H. Lin and R. Che, *J. Mater. Chem. C*, 2014, **2**, 5216-5222.

5. T. K. Gupta, B. P. Singh, S. R. Dhakate, V. N. Singh and R. B. Mathur, *J. Mater. Chem. A*, 2013, **1**, 9138-9149.

6. X. Sun, J. He, G. Li, J. Tang, T. Wang, Y. Guo and H. Xue, *J. Mater. Chem. C*, 2013, **1**, 765-777.

7. K. Singh, A. Ohlan, V. H. Pham, B. R, S. Varshney, J. Jang, S. H. Hur, W. M. Choi, M. Kumar, S. K. Dhawan, B.-S. Kong and J. S. Chung, *Nanoscale*, 2013, **5**, 2411-2420.

8. A. Wang, W. Wang, C. Long, W. Li, J. Guan, H. Gu and G. Xu, *J. Mater. Chem. C*, 2014, **2**, 3769-3776.

9. R. C. Che, C. Y. Zhi, C. Y. Liang and X. G. Zhou, *Appl. Phys. Lett.*, 2006, **88**, 033105.

10. C. He, S. Qiu, X. Wang, J. Liu, L. Luan, W. Liu, M. Itoh and K.-i. Machida, *J. Mater. Chem.*, 2012, **22**, 22160-22166.

11. D. Sun, Q. Zou, Y. Wang, Y. Wang, W. Jiang and F. Li, *Nanoscale*, 2014, **6**, 6557-6562.

12. H. Guo, Y. Zhan, Z. Chen, F. Meng, J. Wei and X. Liu, *J. Mater. Chem. A*, 2013, **1**, 2286-2296.

13. G. Wang, L. Wang, Y. Gan and W. Lu, *Appl. Surf. Sci.*, 2013, **276**, 744-749.

14. Z. Li, B. Shen, Y. Deng, L. Liu and W. Hu, *Appl. Surf. Sci.*, 2009, **255**, 4542-4546.

15. Y. Deng, X. Liu, B. Shen, L. Liu and W. Hu, *J. Magn. Magn. Mater.*, 2006, **303**, 181-184.

16. G. Mu, N. Chen, X. Pan, K. Yang and M. Gu, *Appl. Phys. Lett.*, 2007, **91**, 043110.

17. X.-L. Shi, M.-S. Cao, J. Yuan and X.-Y. Fang, *Appl. Phys. Lett.*, 2009, **95**, 163108.

18. Q. Liu, D. Zhang and T. Fan, *Appl. Phys. Lett.*, 2008, **93**, 013110.

19. M. Cao, H. Lian and C. Hu, *Nanoscale*, 2010, **2**, 2619-2623.

20. G.-X. Tong, W.-H. Wu, Q. Hu, J.-H. Yuan, R. Qiao and H.-S. Qian, *Mater. Chem. Phys.*, 2012, **132**, 563-569.

21. Y. Zhao, H. Pan, Y. Lou, X. Qiu, J. Zhu and C. Burda, *J. Amer. Chem. Soc.*, 2009, **131**, 4253-4261.

22. K. D. Yuan, J. J. Wu, M. L. Liu, L. L. Zhang, F. F. Xu, L. D. Chen and F. Q. Huang, *Appl. Phys. Lett.*, 2008, **93**, 132106.

23. O. O. Otelaja, D.-H. Ha, T. Ly, H. Zhang and R. D. Robinson, *ACS Appl. Mater. Interfaces*, 2014, **6**, 18911-18920.

24. Q. Tian, M. Tang, Y. Sun, R. Zou, Z. Chen, M. Zhu, S. Yang, J. Wang, J. Wang and J. Hu, *Adv. Mater.,* 2011, **23**, 3542-3547.

25. Z. Cheng, S. Wang, Q. Wang and B. Geng, *CrystEngComm*, 2010, **12**, 144-149.

26. T. Zhu, B. Xia, L. Zhou and X. Wen Lou, *J. Mater. Chem.*, 2012, **22**, 7851-7855.

27. R. Cai, J. Chen, J. Zhu, C. Xu, W. Zhang, C. Zhang, W. Shi, H. Tan, D. Yang, H. H. Hng, T. M. Lim and Q. Yan, *J. Phys. Chem. C*, 2012, **116**, 12468-12474.

28. Y.-K. Hsu, Y.-C. Chen and Y.-G. Lin, *Electrochimica Acta*, 2014, **139**, 401-407.

29. J. Kundu and D. Pradhan, *ACS Appl. Mater. Interfaces*, 2014, **6**, 1823-1834.

30. W. He, H. Jia, X. Li, Y. Lei, J. Li, H. Zhao, L. Mi, L. Zhang and Z. Zheng, *Nanoscale*, 2012, **4**, 3501-3506.

31. M. Tanveer, C. Cao, I. Aslam, Z. Ali, F. Idrees, W. S. Khan, M. Tahir, S. Khalid, G. Nabi and A. Mahmood, *New J. Chem.,* 2015, **39**, 1459-1468.

32. K. V. Singh, A. A. Martinez-Morales, K. N. Bozhilov and M. Ozkan, *Chem. Mater*, 2007, **19**, 2446-2454.

33. Y.-Z. Wei, G.-S. Wang, Y. Wu, Y.-H. Yue, J.-T. Wu, C. Lu and L. Guo, *J. Mater. Chem. A*, 2014, **2**, 5516-5524.

34. S. He, G.-S. Wang, C. Lu, J. Liu, B. Wen, H. Liu, L. Guo and M.-S. Cao, *J. Mater. Chem. A*, 2013, **1**, 4685-4692.

35. X.-J. Zhang, G.-S. Wang, Y.-Z. Wei, L. Guo and M.-S. Cao, *J. Mater. Chem. A*, 2013, **1**, 12115-12122.

36. J.-X. Cui, W.-S. Wang, L. Zhen, W.-Z. Shao and Z.-L. Chen, *CrystEngComm*, 2012, **14**, 7025-7030.

37. J. Wang, E. Khoo, P. S. Lee and J. Ma, *J. Phys. Chem. C*, 2008, **112**, 14306-14312.

38. W.-S. Wang, L. Zhen, C.-Y. Xu, J.-Z. Chen and W.-Z. Shao, *ACS Appl. Mater. Interfaces*, 2009, **1**, 780-788.

39. S. Vaidya, P. Rastogi, S. Agarwal, S. K. Gupta, T. Ahmad, A. M. Antonelli, K. V. Ramanujachary, S. E. Lofland and A. K. Ganguli, *J. Phys. Chem. C*, 2008, **112**, 12610-12615.

40. B. Liu, S.-H. Yu, L. Li, Q. Zhang, F. Zhang and K. Jiang, *Angew. Chem. Int. Ed.*, 2004, **43**, 4745-4750.

41. C. Gong, J. Zhang, C. Yan, X. Cheng, J. Zhang, L. Yu, Z. Jin and Z. Zhang, *J. Mater. Chem.*, 2012, **22**, 3370-3376.

42. H.-L. Zhu, Y.-J. Bai, R. Liu, N. Lun, Y.-X. Qi, F.-D. Han and J.-Q. Bi, *J. Mater. Chem.*, 2011, **21**, 13581-13587.

43. L. Wang, X. Jia, Y. Li, F. Yang, L. Zhang, L. Liu, X. Ren and H. Yang, *J. Mater. Chem. A*, 2014, **2**, 14940-14946.

44. B. Zhao, G. Shao, B. Fan, W. Li, X. Pian and R. Zhang, *Mater. Lett*, 2014, **121**, 118-121.

45. B. Zhao, G. Shao, B. Fan, W. Zhao and R. Zhang, *RSC Adv.*, 2014, **4**, 57424-57429.

46. W. Li, B. Lv, L. Wang, G. Li and Y. Xu, *RSC Adv.*, 2014, **4**, 55738-55744.

47. X. Liu, D. Geng, H. Meng, P. Shang and Z. Zhang, *Appl. Phys. Lett*, 2008, **92**, 173117.

48. P. Xu, X. Han, C. Wang, D. Zhou, Z. Lv, A. Wen, X. Wang and B. Zhang, *J. Phys. Chem. B*, 2008, **112**, 10443-10448.

49. X.-L. Shi, M.-S. Cao, J. Yuan, Q.-L. Zhao, Y.-Q. Kang, X.-Y. Fang and Y.-J. Chen, *Appl. Phys. Lett.*, 2008, **93**, 183118.

50. Q. Hu, G. Tong, W. Wu, F. Liu, H. Qian and D. Hong, *CrystEngComm*, 2013, **15**, 1314-1323.

51. R. F. Zhuo, H. T. Feng, J. T. Chen, D. Yan, J. J. Feng, H. J. Li, B. S. Geng, S. Cheng, X. Y. Xu and P. X. Yan, *J. Phys. Chem. C*, 2008, **112**, 11767-11775.

52. H. Li, Y. Huang, G. Sun, X. Yan, Y. Yang, J. Wang and Y. Zhang, *J. Phys. Chem. C*, 2010, **114**, 10088-10091.

53. P. C. P. Watts, W. K. Hsu, A. Barnes and B. Chambers, *Adv. Mater.*, 2003, **15**, 600-603.

54. G. Tong, J. Yuan, W. Wu, Q. Hu, H. Qian, L. Li and J. Shen, *CrystEngComm*, 2012, **14**, 2071-2079.

55. Z. Yang, Z. Li, L. Yu, Y. Yang and Z. Xu, *J. Mater. Chem. C*, 2014, **2**, 7583-7588.

56. X. Chen, F. Meng, Z. Zhou, X. Tian, L. Shan, S. Zhu, X. Xu, M. Jiang, L. Wang, D. Hui, Y. Wang, J. Lu and J. Gou, *Nanoscale*, 2014, **6**, 8140-8148.

57. G. Pan, J. Zhu, S. Ma, G. Sun and X. Yang, *ACS Appl. Mater. Interfaces*, 2013, **5**, 12716-12724.

58. Y. Ren, C. Zhu, S. Zhang, C. Li, Y. Chen, P. Gao, P. Yang and Q. Ouyang, *Nanoscale*, 2013, **5**, 12296-12303.

59. R. Li, T. Wang, G. Tan, W. Zuo, J. Wei, L. Qiao and F. Li, *J. Alloys Compd.*, 2014, **586**, 239-243.

60. C. Wang, X. Han, X. Zhang, S. Hu, T. Zhang, J. Wang, Y. Du, X. Wang and P. Xu, *J. Phys. Chem. C*, 2010, **114**, 14826-14830.

61. B. Zhao, G. Shao, B. Fan, B. Sun, K. Guan and R. Zhang, *J. Mater. Sci.: Mater. Electron.*, 2014, **25**, 3614-3621.

62. S. He, C. Lu, G.-S. Wang, J.-W. Wang, H.-Y. Guo and L. Guo, *ChemPlusChem*, 2014, **79**, 569-576.

63. B. Zhao, G. Shao, B. Fan, W. Zhao, Y. Xie and R. Zhang, *RSC Adv.*, 2014, **4**, 61219-61225.

64. B. Zhao, G. Shao, B. Fan, C. Wang, Y. Xie and R. Zhang, *Powder Technol.*, 2015, **270,** , 20-26.

65. P. H. Fang, *J. Chem. Phys.s*, 1965, **42**, 3411-3413.

66. W. Pan, Q. Liu, R. Han, X. Chi and J. Wang, *Appl. Phys. A*, 2013, **113**, 755-761.

67. N. Ortega, A. Kumar, R. Katiyar and C. Rinaldi, *J. Mater. Sci.* 2009, **44**, 5127-5142.

68. S. Wen, Y. Liu, X. Zhao, J. Cheng and H. Li, *J. Magn. Magn. Mater.*, 2014, **354**, 7-11.

69. R. F. Zhuo, H. T. Feng, Q. Liang, J. Z. Liu, J. T. Chen, D. Yan, J. J. Feng, H. J. Li, S. Cheng, B. S. Geng, X. Y. Xu, J. Wang, Z. G. Wu, P. X. Yan and G. H. Yue, *J. Phys. D: Appl. Phys.*, 2008, **41**, 185405.

70. G. Li, T. Xie, S. Yang, J. Jin and J. Jiang, *J. Phys. Chem. C*, 2012, **116**, 9196-9201.

71. B. Zhao, G. Shao, B. Fan, Y. Xie, B. Sun and R. Zhang, *Adv. Powder Technol.*, 2014, **25**, 1761-1766.

Graphical Abstract

The flower-like CuS hollow microspheres exhibit the advantages of strong absorption, thin thickness, wide band and light weight.